Title

Expression patterns of CYP26A1, FGF8, CDKN1A, and NPVF in the developing rhesus monkey retina

Authors

Krueger, Miranda R

Fishman-Williams, Elizabeth

Simó, Sergi

et al.

Publication Date

2024

DOI

10.1016/j.diff.2023.100743

Peer reviewed

HHS Public Access

Author manuscript

Differentiation. Author manuscript; available in PMC 2024 February 15.

Published in final edited form as:

Differentiation. 2024 ; 135: 100743. doi:10.1016/j.diff.2023.100743.

Expression patterns of *CYP26A1, FGF8, CDKN1A*, and *NPVF* in the developing rhesus monkey retina

Miranda R. Krueger[a,1], **Elizabeth Fishman-Williams**[a,1], **Sergi Simó**[a], **Alice F. Tarantal**[a,b,c], **Anna La Torre**[a,*]

[a]Department of Cell Biology and Human Anatomy, University of California, Davis, Davis, CA, 95616, United States

[b]Department of Pediatrics, University of California, Davis, Davis, CA, 95616, United States

[c]California National Primate Research Center, University of California, Davis, Davis, CA, 95616, United States

Abstract

The *fovea centralis* (fovea) is a specialized region of the primate retina that plays crucial roles in high-resolution visual acuity and color perception. The fovea is characterized by a high density of cone photoreceptors and no rods, and unique anatomical properties that contribute to its remarkable visual capabilities. Early histological analyses identified some of the key events that contribute to foveal development, but the mechanisms that direct the specification of this area are not understood. Recently, the expression of the retinoic acid-metabolizing enzyme *CYP26A1* has become a hallmark of some of the retinal specializations found in vertebrates, including the primate fovea and the high-acuity area in avian species. In chickens, the retinoic acid pathway regulates the expression of *FGF8* to then direct the development of a rod-free area. Similarly, high levels of *CYP26A1, CDKN1A,* and *NPVF* expression have been observed in the primate macula using transcriptomic approaches. However, which retinal cells express these genes and their expression dynamics in the developing primate eye remain unknown. Here, we systematically characterize the expression patterns of *CYP26A1, FGF8, CDKN1A*, and *NPVF* during the development of the rhesus monkey retina, from early stages of development in the first trimester until the third trimester (near term). Our data suggest that some of the markers previously proposed to be fovea-specific are not enriched in the progenitors of the rhesus monkey fovea. In contrast, *CYP26A1* is expressed at high levels in the progenitors of the fovea, while it localizes in a subpopulation of macular Müller glia cells later in development. Together these data provide invaluable insights into the expression dynamics of several molecules in the nonhuman primate retina and highlight the developmental advancement of the foveal region.

[*]Corresponding author. Department of Cell Biology and Human Anatomy School of Medicine University of California, Davis One Shields Avenue, 3402 Tupper Hall Davis, CA, 95616, United States. alatorre@ucdavis.edu (A. La Torre).

[1]These authors contributed equally to this work.

Appendix A. Supplementary data

Supplementary data to this article can be found online at https://doi.org/10.1016/j.diff.2023.100743.

Keywords

Foveal development; Retinal development; CYP26A1; FGF8; NPVF

1. Introduction

Sight is our most important sense and has provided us with an unparalleled evolutionary advantage for complex tasks, such as decision making, attention, and memory. Vision begins at the retina, an intricate laminar structure that lines the back of the eye (Dowling, 1987). The retina detects light and converts it to neural signals that are then relayed to the visual centers of the brain. To accomplish these functions, the retinal layers contain diverse and specialized sets of cellular populations, including sensory receptors (rod and cone photoreceptors), projection neurons (retinal ganglion cells, RGCs), interneurons (horizontal cells, bipolar cells, and amacrine cells), and a population of glia (Müller glia) (Kolb, 1995). It is well established that during development, a single population of multipotent progenitor cells produces these seven main retinal cell types (Holt et al., 1988; Turner and Cepko, 1987). Moreover, the sequential birth order of these cells is conserved across all vertebrate species, such that RGCs, cones, horizontal cells, and GABAergic amacrine cells are born first, while other amacrine populations, rod photoreceptors, bipolar cells, and Müller glia are generated later during the period of neurogenesis (La Vail et al., 1991; Rapaport et al., 2004; Sidman, 1961; Wallace, 2011; Young, 1985; Zhang et al., 2023).

Despite this conservation, there are species-specific retinal differences due to visual necessities, behaviors, and habitats, namely variations in the ratios of different cell types and populations (Baden, 2020; Viets et al., 2016). Even within a single retina, specialized regions with distinct cell compositions exist. The primate *fovea centralis* (fovea) is one such example of a specialized retinal region, where cone photoreceptors are the dominant cell population in a sharp contrast to the majority of the retina where rods outnumber cones 20:1 (Curcio et al., 1987, 1990). Located at the center of the *macula lutea* (macula), slightly temporal to the optic disk, the fovea contains a particularly high number of densely-packed cone photoreceptors, organized in a bouquet-like spatial arrangement, and no rods (Curcio et al., 1987, 1990; Kolb et al., 1995). Other differences between the macula and the neighboring retina include a different ratio of photoreceptors to RGCs, the output neurons of the retina. The ratio of cones to RGCs in the fovea can be 1:3 (Sjostrand et al., 1999), whereas outside the fovea, there is convergence of signals from many photoreceptors onto one RGC. This adaptation results in a higher concentration of RGCs in the macula, such that a region that occupies only 0.002% of the total retinal surface contains 25% of all RGCs (Curcio and Allen, 1990). Additionally, the fovea develops into a pitted invagination by peripherally displacing the inner retinal layers (Hendrickson and Kupfer, 1976; Hendrickson et al., 2012; Provis et al., 1998). Together with the lack of blood vessels (foveal avascular zone (Gariano et al., 2000; Provis and Hendrickson, 2008)), these specializations minimize light scattering and provide the fovea with the highest visual resolution of the retina.

Even though the development of the retina has been well studied, the mechanisms governing the development of the fovea have remained largely unexplored, mostly due to the lack of

a fovea in small animal model organisms. Gaining understanding into the factors governing how the fovea develops is not only critical for unraveling the fundamental principles of retinal development, but also holds tremendous potential for therapeutic strategies aimed at combating retinal diseases and restoring vision.

Besides primates, birds of prey and lizards also have high-acuity vision and foveated retinas (Mitkus et al., 2017; Rasys et al., 2021; Roll, 2001; Sannan et al., 2018), and other species, including chickens and zebrafish, have retinal specializations with the features of a high-acuity area (HAA) (da Silva and Cepko, 2017; Yoshimatsu et al., 2020). Using some of these models, the retinoic acid (RA) pathway has been proposed as a key regulator of foveal development. RA is an active derivative of vitamin A, and its spatial and temporal distributions result from the regulated expression of RA-synthesizing retinaldehyde dehydrogenases (RALDHs) and RA-metabolizing cytochrome P450s (CYP26) enzymes. Together with FGF8, CYP26A1 expression is an early distinctive feature of the chick HAA, and, in fact, the expression of FGF8 regulated by RA seems to be a requirement for the development of a rod-free region in avian species (da Silva and Cepko, 2017). Notably, transcriptomic approaches using human (Lu et al., 2020) and nonhuman primate (rhesus monkey) (Fishman et al., 2021) samples have also shown high levels of expression of *CYP26A1* in the developing macula, underscoring its potential roles in foveal development. These studies have also identified other genes with higher expression rates in the developing temporal retina, including *NPVF* and *CDKN1A* ($P21^{CIP1}$). However, their expression patterns in the developing primate retina have yet to be described.

Here, we have investigated the expression dynamics of *CYP26A1, FGF8, NPVF*, and *CDKN1A* at different developmental stages using the rhesus monkey model (*Macaca mulatta*). The rhesus monkey offers unique advantages, as it shares most of the features of human vision, including our high-resolution central vision (Picaud et al., 2019), and it is possible to obtain samples across all stages of gestation. Our data indicate that some of the markers transcriptionally enriched in the fovea at early stages of development are expressed by Müller glia cells, highlighting the developmental advancement of this region, but these markers are not fovea-specific at later stages of development. We also show that *CYP26A1* exhibits high expression levels in the progenitors of the fovea, albeit its expression is not limited to this region at early stages, while at later stages of development, this gene is restricted to the Müller glia cells of the macula. Together, these data underscore the stark advances of the foveal area in comparison to the rest of the retina and suggest that the foveal Müller glia could have unique molecular signatures.

2. MATERIALS and METHODS

2.1. Sample collection

All animal procedures conformed to the requirements of the Animal Welfare Act and protocols were approved prior to implementation by the Institutional Animal Care and Use Committee (IACUC) at the University of California at Davis. Healthy adult female rhesus monkeys (*Macaca mulatta*) were time-mated and identified as pregnant using established methods (Tarantal 2005). Pregnancy in the rhesus monkey is divided into trimesters by 55-day increments: 0–55 days gestational age represents the first trimester, 56–110 days

represents the second trimester, and 111–165 days the third trimester (term 165 ± 10 days). Normal fetal growth and development were confirmed by ultrasound during gestation (Tarantal, 2005). Dams were scheduled for hysterotomy (*e.g.,* approximately 40, 50, 60, 75, 80, 110, 140, and 145 days gestational age; all gestational ages ±2 days based on timed mating protocol) for fetal tissue collection. Gestational percentages (Table 1) are 24% and 30% gestation (1st trimester), 36%, 42%, and 65% gestation (2nd trimester), and 85% and 88% gestation (3rd trimester). For each time point we collected at least two samples with the early stage (40 days gestational age) and later stage (140 days gestational age) represented by three samples. Dams were returned to the breeding colony post-hysterotomy.

The fetal eyes were collected into cold media (DMEM and FBS) then extraneous tissue was removed and the retina was incubated in oxygenated media for 90 min at room temperature. Samples were then fixed in modified Carnoy's fixative (ethanol, formaldehyde, and acetic acid) overnight at 4 °C, dehydrated in stepwise ethanol/water solutions, cleared with xylene, and embedded in paraffin blocks. Retinas were sectioned (6 μm) on a horizontal plane and were stored in open slide boxes at room temperature before subsequent staining.

For all comparisons between nasal and foveal regions, the nasal area was selected at the same distance from the optic nerve head as the presumptive fovea (also referred as temporal).

2.2. RNAscope in situ hybridization and immunohistochemistry

RNAscope detection was performed according to the RNAscope Multiplex Fluorescent Reagent Kit v2 Assay manual. Following sample fixation and preparation described above, sections were treated with heat and three pretreatment steps: After baking for 1 h at 60 °C and deparaffinizing with xylene and ethanol, sections were pretreated with hydrogen peroxide for 10 min at room temperature, target retrieval for 15 min at 99 °C, and protease plus for 30 min at 40 °C. Sections were incubated with the appropriate hybridization probes for 2 h at 40 °C, followed by a series of amplification steps and fluorescent labeling with Opal dyes (Opal 520 and 620), as per manufacturer instructions. After the final wash buffer step in the RNAscope protocol, we began an immunohistochemistry protocol to combine the RNA *in situ* with antibody staining. Sections were incubated in PBS for 5 min and blocked in 10% normal donkey serum/PBS-0.1% Triton X-100 for 1 h at room temperature. Primary antibodies were diluted in blocking solution for an overnight incubation at 4 °C. After primary antibody incubation, sections were washed five times (5 min each) in PBS. Species-specific, fluorescently labeled secondary antibodies (Invitrogen, 1:200) were diluted in blocking solution for a 1 h incubation at room temperature. Cell nuclei were counterstained with 4',6-diamidino-2-phenylindole (DAPI, Sigma-Aldrich). The sections were rinsed five times (5 min each) in PBS and mounted for microscopy using a Fluoromount-G (Southern Biotech). See table below for details of antibodies and working dilutions. Images were taken using a Fluoview FV3000 confocal microscope (Olympus) or Axio Imager.M2 with Apotom.2 microscope system (Zeiss). All images were assembled using Photoshop and Illustrator (Adobe).

Antibody	Source	Catalog	Lot	Concentration
Anti-ATOH7 (Rabbit)	Novus Biological	88639	A106752	1:200
Anti-BRN3 (Goat)	Santa Cruz	sc-6026	H2416	1:100
Anti-CRX (Mouse)	Abnova	H00001406-M02	KB191–4G11	1:200
Anti-Glutamine Synthetase (Mouse IgG2a)	Millipore	MAB302	3821584	1:150
Anti-LHX4 (Rabbit)	Proteintech	11183–1AP	00040977	1:200
Anti-NRL (Goat)	R&D Systems	AF2945	VYM032002A	1:400
Anti-OTX2 (Goat)	R&D Systems	AF1979	KRS0320091	1:200
Anti-PAX6 (Rabbit)	Bio Legend	901301	B386304	1:200
Anti-PCNA (Rabbit)	Abcam	AB18197	GR3262110–2	1:100
Anti-PH3 (Rabbit)	Thermo Fisher	PA5–17869		1:100
Anti-TUJ1 (Mouse)	BioLegend	801201	B264428	1:500
Anti-RXRgamma (Mouse)	Santa Cruz	sc-365252	D0623	1:200

2.3. Hematoxylin and eosin (H&E) staining

Samples were fixed and prepared as described above. Next, sections were deparaffinized using xylene, rehydrated with stepwise ethanol/water solutions, stained with hematoxylin, rinsed with acid alcohol and ammonia water, counterstained with eosin, and dehydrated in stepwise ethanol/water solutions. Sections were then rinsed with xylene and mounted for microscopy using Permount (Fisher Chemical).

2.4. EdU Click-iT

For 5-Ethynyl-2′-deoxyuridine (EdU) labeling experiments, eyes were incubated in oxygenated media for 90 min, followed by a 2 h incubation of EdU at 5 mg/ml at 40 °C. Eyes were then fixed with modified Carnoy's media (see above), paraffin embedded, and sectioned. Tissue sections were treated with antigen retrieval steps of hot (95 °C) 0.01 M sodium citrate pH 8 twice for 5 min each, followed by an acid treatment (2 N HCl and PBS-0.5% Triton X-100/PBS) for 1 h at room temperature in a humidifying chamber. EdU was then detected following the manufacturer instructions (Thermo Fisher Scientific, C10337). RNAscope *in situs* (protocol above) were performed in combination with Edu Click-it kit staining. Here, the EdU protocol was initiated after the final wash buffer steps of the *in situ* protocol. In this case, we did not perform the sodium citrate antigen retrieval.

2.5. Statistical methods

Quantifications of retinal length were obtained for each side of the retina (temporal and nasal) from the ONH to the ora serrata using three biological replicates. Mean and P-values were obtained using the Student's T-test. Similarly, the ganglion cell layer thickness was quantified at the foveal center and at the equivalent distance from the optic nerve head in the nasal side from three biological replicates at 40 days gestational age (first trimester). Student's T-test was used to obtain mean and P-values. All statistical analyses and plot generation was performed using Prism 9 (GraphPad).

3. Results

3.1. Neurogenesis in the developing rhesus retina follows a fovea-to-periphery gradient

Fetal rhesus monkey samples spanning the three trimesters of gestation were analyzed using H&E staining (Table 1). We analyzed samples from the first trimester (~40 days) to the late third trimester (140 days gestational age; term 165 ± 10 days). These experiments revealed the asymmetry of the developing retina from 40 days gestational age (~24% gestation), where the temporal region is larger (1.93-fold larger, *p*-value: 0.001, Fig. 1A–B, Table 1) and shows a wider ganglion cell layer (GCL) (Fig. 1C, *p*-value: 0.011 and Fig. 1D). We also observed a clear developmental advancement of the foveal region, evidenced by an earlier presence of plexiform layers in the foveal region compared to the equidistant region from the ONH in the nasal region (Fig. 1E–P). By 50 days gestational age (~30% gestation), the inner plexiform layer (IPL) begins to develop at the center of the foveal anlage, and by 60 days (~36% gestation), the IPL is distinct in the temporal retina but not yet in the nasal retina (Fig. 1F–G, L-M, arrows). Similarly, by 80 days gestational age (second trimester, ~48% gestation) the IPL is well-defined across the entire retina, with the initial presence of the outer plexiform layer (OPL) only in the foveal region (Fig. 1H, N). By 110 days (beginning of the third trimester, ~67% gestation), the foveal pit has started to develop into a shallow depression that already exhibits some lateral RGC displacement (Fig. 1D, Q, Table 1). At 140 days gestational age (~85% gestation), the fovea consists of a deep invagination and part of the GCL has displaced peripherally, as revealed by a thinner GCL at the foveal center (1–2 cells thickness, Fig. 1D and S, Table 1). However, the inner nuclear layer (INL) still maintains a uniform thickness between the pit region and the surrounding retina (Fig. 1S). Similar regions in the nasal side do not present these modifications (Fig. 1R, T). Immunohistochemistry confirmed that while the majority of CRX + photoreceptors are NRL + rods throughout the retina, we did not detect NRL + cells at the center of the foveal pit, indicating the predominance of cone photoreceptors in this region (Fig. 1U–V″).

A switch from early to late progenitor competence takes place in the late first trimester at 50 days gestational age in the center of the fovea.

We used cell-specific antibodies to evaluate neurogenesis of different retinal populations. Recent analyses have revealed a distinct shift in retinal progenitor cells (RPCs) consistent with their competence to generate early-(*e.g.,* RGCs and cones) versus late-born retinal cell types (*e.g.,* bipolar cells and Müller glia). Early and late RPCs express distinct transcriptional signatures, and single cell “omics” have distinguished broad transitions in RPCs at embryonic day 16 (E16) in mice and between 11 and 15 gestational weeks in humans (Clark et al., 2019; Lu et al., 2020; Sridhar et al., 2020).

At the earliest stage analyzed (40 days gestational age), we observed BRN3+ TUJ1+ RGCs in the apical side throughout the retina (Fig. 2A–B′, arrows). RPCs divide at the apical side of the retina and as a result, newly born postmitotic neurons need to migrate basally to their appropriate layers. Thus, the presence of BRN3+ TUJ1+ cells in the apical region indicates active RGC neurogenesis. By 50 days, most of the RGCs are localized in the GCL in the temporal side of the retina, suggesting that RGC genesis is completed in the fovea (Fig.

2C–C'). In contrast, we still detected many BRN3+ RGCs in the most apical part of the retina in the nasal region (Fig. 2D, arrows).

The basic-helix-loop-helix (bHLH) transcription factor ATOH7 plays a critical role in early neurogenesis, and while ATOH7+ progenitors can generate all different cell types, it is necessary for the generation of RGCs (Brown et al., 1998; Brzezinski et al., 2012). Its expression starts during the final cell division of RPCs and follows a highly-regulated expression pattern that coincides with the first wave of neurogenesis. In mouse retinas, Atoh7 expression initiates at E11, peaks at E14.5, and rapidly decreases after E16.5 (Miesfeld et al., 2018). In the rhesus monkey retina, ATOH7 is downregulated first at the center of the fovea at 40 days gestational age, later extending within the temporal side (Fig. 2E–F′). By 50 days, ATOH7 is not detected in the foveal region by immunohistochemistry, but ATOH7 expression still remains expressed elsewhere within the same retina (Fig. 2G–H′). Similarly, we observe RXRgamma + photoreceptors (presumptively cone photoreceptors) first in the temporal retina. By 40 days gestational age, we observe RXRg + photoreceptors in the foveal region, but only at 50 days, we observe RXRg + photoreceptors across all regions (Fig. 2 I–L').

Correspondingly, at this stage, LHX4+ OTX2+ bipolar cells and *RLBP1*+ Müller glia are detected only in the center of the fovea, indicating that by end of the first trimester (50 days gestational age), foveal RPCs are producing late cell types (Fig. 3). Previous studies have identified LHX4 expression in cone photoreceptors (Buenaventura et al., 2019) and therefore, to further validate that the LHX4+ cells detected at 50 days are indeed bipolar cells, we assessed the expression of LHX4 and OTX2 at different developmental stages (Supplementary Fig. 1). By 75 days gestational age, we only detected LHX4+ cells in the INL (bipolar cells) and not in OTX2+ cells of the ONL (photoreceptors). By 110 days (beginning of the third trimester), we begin to see LHX4+ cone photoreceptors at the apical side of the ONL in the temporal side, but its expression remains constrained to the INL in the nasal side. These data suggest that LHX4 is expressed in bipolar cells at early stages of development, and only at later stages of maturation is it expressed in cones.

We also analyzed the presence of mitotic cells using phospho-Histone3 (PH3) immunostaining (Supplementary Fig. 2). At 50 days gestational age, we detected mitotic cells across the retina, but from 60 days onward, we no longer observed PH3+ cells in the center of the foveal region. As development proceeds, the absence of PH3 extended peripherally, but by 80 days gestational age, we still detected PH3+ mitotic RPCs in the nasal side of the retina. By the late third trimester (140 days gestational age), we only detected a few mitotic cells in the ciliary margin, nor did we observe PH3+ RPCs in either side of the retina.

As summarized in Table 1, these data indicate that the fovea is developmentally advanced compared to the rest of the retina and that neurogenesis takes places in a wave that begins in the center of the fovea and extends towards the periphery. Our results also indicate that a shift between early and late RPC competence states takes place in the late first trimester (around 50 days gestational age) in the rhesus monkey fovea.

CYP26A1 is highly expressed in the developing rhesus monkey fovea at different stages of development.

In order to describe the expression pattern of genes previously proposed to be enriched in foveal RPCs, we used RNAscope *in situ* hybridization (Advanced Cell Diagnostics). In our experiments, the background levels detected with this method are very low (Supplementary Fig. 3).

At 40 days gestational age, the earliest time-point analyzed, *CYP26A1* is highly enriched in the developing fovea and only expressed at low levels in the nasal region (Fig. 4A–B′). We also detected *CYP26A1* expression in RPCs surrounding the optic nerve head (ONH, Fig. 4A–B′), in the ciliary marginal zone, and in the lens epithelium (Fig. 4A–A′, Table 2). The cells that expressed the highest levels of *CYP26A1* are PCNA+ (Fig. 4B–B′, Supplementary Fig. 4A–A″) and some colocalize with EdU (Supplementary Fig. 4B–C″), indicating that *CYP26A1* is expressed by RPCs. However, even within the foveal anlage, not every EdU + cell expressed *CYP26A1*. We did not detect colocalization with OTX2+ photoreceptors nor any expression in the GCL, suggesting that CYP26A1 is not expressed in photoreceptors or RGCs (Supplementary Fig. 4D–D″, Table 2). This expression remains unchanged at 50 days, where the foveal RPCs and a small patch of cells bordering the ONH exhibit the highest levels of *CYP26A1* (Fig. 4, Table 2).

At later stages of development, *CYP2*6A1 expression is restricted to the Müller glia (Fig. 5). The Müller glia of the fovea and macula regions (including the foveal center, parafovea and part of the perifovea) express high levels of *CYP26A1*, but this gene is not expressed by the Müller glia of other parts of the retina (Fig. 5A–D). Thus, *CYP26A1* colocalizes with *RLBP1* (also known as *CRALBP*), a robust marker of Müller glia cells (Vazquez-Chona et al., 2009), and glutamine synthetase (GS, Fig. 5E–E‴ and Supplementary Fig. 5A–A‴).

3.2. FGF8 is expressed in retinal progenitors in a ONH-to-periphery gradient

In avian species, the RA pathway regulates the expression of *FGF8*, which serves as a molecular marker for the HAA throughout development (Amamoto et al., 2019; Yamagata et al., 2021). We investigated whether this expression is conserved in primates using RNAscope *in situ* hybridization. In contrast with the known expression pattern in chickens, in the early developing rhesus monkey retina, the highest levels of *FGF8* were found localized around the ONH and diffuse in a gradient peripherally (Fig. 6A, Table 2). Co-labeling experiments using *FGF8* and *CYP26A1* showed distinct expression patterns for these two genes (Fig. 6. A′). This pattern of expression remained unaltered at 50- and 70-days gestational age (Fig. 6B–G′). At later stages of development, *FGF8* is only detected at low levels of expression in both the ONL and INL, but not in other eye tissues (Fig. 6. H–J', Table 2).

3.3. CDKN1A is expressed by the Müller glia and ONH cells

Previous experiments have identified *CDKN1A* ($p21^{CIP1}$) as a gene enriched in the temporal region of the retina from 50 to 150 days gestational age in rhesus monkeys (Fishman et al., 2021) and in human fetal week 20 samples (Lu et al., 2020). *CDKN1A* was also found in a study aimed at identifying cone-specific transcriptional signatures (Buenaventura et al.,

2019). $p21^{CIP1}$ and $p27^{XIC1}$ are G1-checkpoint CDK inhibitors, and thus, we investigated the intriguing possibility that *CDKN1A* could be enriched in foveal RPCs and/or cone photoreceptors.

RNAscope *in situ* hybridization did not detect expression of *CDKN1A* at 40 days gestational age, but by 50 days, our analyses revealed *CDKN1A* expression in the center of the foveal anlage as well as in the optic nerve head (ONH, Fig. 7A–A″ arrows, Table 2). This expression colocalized with *RLBP1*. The expression of *CDKN1A* extended peripherally as time progressed and by 75 days, it has extended throughout the temporal retina (Fig. 7E–E′). At this stage of development, we still detected high levels of expression in the ONH (Fig. 7F–F′, arrow). By the late third trimester, we observed CDKN1A throughout the whole retina and its expression remained restricted to *RLBP1*+ Müller glia cells in both the temporal and nasal sides of the retina (Fig. 7H–J'). Together, these data suggest that *CDKN1A* is expressed by Müller glia cells throughout development in the rhesus monkey.

3.4. The neuropeptide NPVF is expressed by the Müller glia

Similarly, *NPVF* (Neuropeptide VF precursor) was previously found to be enriched in the temporal primate retina (Fishman et al., 2021; Lu et al., 2020). *NPVF* is expressed by the hypothalamus and regulates sleep in some species (Lee et al., 2017). Expression of *NPVF* was previously correlated with retina aging (Yi et al., 2021), but the pattern of expression during development has not been explored.

Using RNAscope *in situ* hybridization, we observed *NPVF* expression beginning at approximately 50 days gestational age (Fig. 8). At this stage, *NPVF* is only expressed by a few cells at the center of the macula. The expression of *NPVF* extends laterally as time proceeds and colocalizes with *RLBP1* and GS, indicating that this gene is expressed by the Müller glia, possibly at somewhat later developmental stages when compared to *CDKN1A* expression (Fig. 8, Table 2).

4. Discussion

In the study described herein, we have characterized key morphological characteristics of the developing rhesus monkey fovea, the timing of neurogenesis, and the expression patterns of *CYP26A1, FGF8, NPVF*, and *CDKN1A* at different ontogenic stages.

We have shown that the embryonic retina undergoes asymmetrical growth, exhibiting a larger temporal region, where the incipient fovea resides (Fig. 1). This observation mimics published histological images that show that, while the optic cup is symmetrical in its temporal-nasal axis by 30 days gestational age, the temporal side of the optic cup is much larger than the nasal side from 36 days onward (Townes-Anderson and Raviola, 1981). We also observed a thicker GCL in the temporal side at 40 days (24% of gestation) and a clear developmental advancement of the foveal region, as the plexiform layers appear first in the center of the fovea before extending towards the periphery. The foveal pit is initially a shallow depression that can be observed by 110 days gestational age (65% of gestation) and then develops into a deeper pit. The development of the pit takes place in conjunction with a

lateral displacement of the GCL, similar to prior descriptions in other morphological studies (Hendrickson, 1992).

Foundational studies by Hendrickson (Hendrickson, 1992; Hendrickson and Kupfer, 1976; Okada et al., 1994), Provis (Cornish et al., 2005), and Rakic (La Vail et al., 1991; Wikler and Rakic, 1991), and more recently transcriptomic approaches (Finkbeiner et al., 2022; Fishman et al., 2021; Lu et al., 2020; Sridhar et al., 2020; Thomas et al., 2022) have revealed changes in differentiation and maturation rates between the fovea and the rest of the retina. For instance, late-born cell types, such as bipolar cells and Müller glia, are found in the fovea at much earlier developmental stages compared to the nasal retina (Fishman et al., 2021; Hoshino et al., 2017; La Vail et al., 1991). Correspondingly, progenitors exit the cell cycle much sooner in the foveal region (Dyer et al., 2009; Fishman et al., 2021; Hoshino et al., 2017). Classic studies from La Vail, Rapaport, and Rakic (La Vail et al., 1991) used ^{3}H-thymidine labeling at different times during development to define the timing of cell genesis in the rhesus monkey retina. Since these analyses were performed at later stages, several factors could be confounding the data: (1) significant retinal growth takes place after neurogenesis and thus passive cell movements to accompany organ growth could have occurred between cell birth and sample collection, (2) active cell movements towards and away from the fovea have been described during pit formation (Bringmann et al., 2018; Hendrickson and Kupfer, 1976; Hendrickson and Yuodelis, 1984; Yuodelis and Hendrickson, 1986), (3) all the analyses were performed after the period of cell death and RGC culling (Rakic and Riley, 1983), and (4) all the analyses were based on cell position but no specific markers were used.

In the La Vail dataset, the onset of neurogenesis was defined at ~30 days gestational age, when the first RGCs and horizontal cells are born in the foveal center. The onset of cone genesis was found at ~33 days, and the onset of genesis of late cell types was identified at ~45 days. This study describes a pronounced fovea-to-periphery gradient of cytogenesis. Similarly, *in silico* predictions have been recently used to estimate the onset of neurogenesis for different retinal cell populations (Fishman et al., 2021). These calculations estimate RGC genesis to begin around 33 days, rod bipolar genesis onset to be ~52 days, and bipolar cell genesis to begin at ~55 days gestational age. To shed light on the timing of cell birth in rhesus monkeys, we have explored neurogenesis during the embryonic period. Our data suggest that RGC genesis begins prior to 40 days and is completed by 50 days in the foveal center (Fig. 2), while bipolar cells and Müller glia are found in the center of the foveal anlage by 50 days (late first trimester) (Fig. 3). ATOH7, a transcription factor dynamically expressed in subsets of RPCs and required for RGC formation (Brown et al., 1998; Brzezinski et al., 2012; Miesfeld et al., 2018), is downregulated from the fovea by day 50. Together these data validate the dataset published by La Vail and indicate that the shift between early and late competence periods takes place at the end of the first trimester in the primate fovea.

Through the advent of high-throughput sequencing technologies, our understanding of primate retina cell types and their gene expression profiles has broadened (Peng et al., 2019; Yan et al., 2020; Yi et al., 2021), spurring the search for reliable foveal markers and the complementing mechanisms driving foveal development. Notably, the RA catabolizing

enzyme *CYP26A1* has been previously identified as a foveal marker in several studies (da Silva and Cepko, 2017; Fishman et al., 2021; Lu et al., 2020; Peng et al., 2019), and a pathway involving CYP26A1 and FGF8 is required for the patterning of the HAA in chickens (da Silva and Cepko, 2017). Our data indicate that *CYP26A1* is highly enriched in primate foveal RPCs, although we also detected some levels of *CYP26A1* expression in other regions of the eye. Contrarily, *FGF8* is not enriched in the developing fovea at any of the gestational ages analyzed. These expression patterns suggest that RA-dependent patterning could be an important aspect regulating the development of the fovea and high acuity areas across species, but the exact molecular mechanism(s) downstream may not be conserved between avian species and primates.

RA is known to participate in dorso-ventral patterning (Marsh--Armstrong et al., 1994) and in mice, *Cyp26A1* and *Cyp26C1* cooperate to establish a stripe of lower RA levels within the equatorial rodent retina (Sakai et al., 2004; Wagner et al., 2000). Alterations in *Cyp26* expression leads to perturbations of the ratios of cone opsins and RGC projection patterns (Sakai et al., 2004). However, mice do not have foveal specialization or rod-free regions, and thus, neither *CYP26A1* expression nor lower levels of RA are sufficient to drive foveal development.

At later times in development, *CYP26A1* is expressed by *RLBP1*+ GS + macular Müller glia, including the Müller glia within the foveola, fovea, parafovea, and part of the perifovea, but *CYP26A1* is not expressed by Müller glia in other parts of the retina. This expression pattern has been observed in the adult rhesus monkey eye (Peng et al., 2019). Similarly, novel findings using the zebrafish model also suggest conserved expression patterns of *cyp26a1* in the Müller glia of the HAA (Lahne and MacDonald, 2023).

Similar to *CYP26A1, CDKN1A* and *NPVF* have been identified in transcriptomic analyses as genes enriched in the developing fovea. In our previous analyses, *NPVF* was shown to have one of the highest enrichments in the temporal retina compared to the nasal retina (420-fold enrichment at 90 days gestational age). *CDKN1A* showed 11.7-fold enrichment in the temporal side, comparable to the 17.9-fold enrichment exhibited by *CYP26A1* at the same developmental time point (Fishman et al., 2021). Here, we observed a clear colocalization between both *CDKN1A* and *NPVF* with *RLBP1*, indicating that these molecules are expressed in Müller glia cells. By 50 days gestational age, we observed substantial levels of *CDKN1A* in the temporal retina, while NPVF is only expressed by a few cells in the center of the foveal anlage. As development proceeds, the region that expresses these genes extends peripherally, such that by 140 days gestational age (late third trimester), we observed *CDKN1A* expression in both sides of the retina, while *NPVF* expression had extended in the temporal retina but is only modestly expressed by the Müller glia at the nasal side. Together, these data suggest that these genes are not exclusive of the developing fovea but are instead expressed by Müller glia at different stages of maturation, and that the enriched expression detected in previous studies is associated with the gradient of Müller glia production and maturation.

The presence of different glial cells in the foveal pit remains poorly understood. Early electron microscopy studies (Yamada, 1969) observed “cone-shaped Müller glia” in the

innermost part of the fovea. Gass (1999) revisited these preparations and observed that the cytoplasm composing the outer portion of these Müller cells appeared optically empty, indicating that perhaps the Müller glia of the foveola could have unique properties. More recently, one study has identified GFAP + glial cells in the foveal center but these glia cells do not appear to express RLBP1 or GS (Delaunay et al., 2020). The authors of this study proposed that the glial cells present in the foveal floor are not Müller glia but astrocytes. However, previous primate studies suggest that the avascular zone within the macula remains devoid of astrocytes and vessels at all times (Provis et al., 2000) and thus, the identity of the glia cells of the foveola remains a contentious topic. In our preparations, we observed a reduction in *RLBP1* in the center of the foveal pit at 140 days gestational age (see Fig. 7H' and 8E'). However, we did not observe a corresponding reduction in *CYP26A1, CDKN1A,* or *NPVF*, indicating that Müller glia cells are likely present in this region. Single-cell sequencing studies have reported differences between the glial cells of the fovea and the periphery, but expression of *RLBP1* has been detected in both foveal and peripheral Müller glia (Voigt et al., 2019). However, most "omics" studies analyze the tissue obtained within a 2–3 mm punch and thus, these approaches do not distinguish the center of the fovea from the rest of the macula. The possible reduction of *RBLP1* together with the expression of *CYP26A1* only in the macular Müller glia suggests that the Müller glia of the fovea/macula exhibit some unique molecular signatures.

Taken together, our results demonstrate the spatial and temporal expression patterns of several genes, previously hypothesized to be fovea-specific, and reveal that from all the genes analyzed, only *CYP26A1* is enriched in the fovea across different ontogenic stages. However, the dynamic changes of *CYP26A1* expression in different regions of the retina, and in RPCs and Müller glia may pose challenges to be used as a fovea RPC-specific marker for single-cell approaches.

In the future, by integrating the knowledge obtained from diverse species, including primate, chickens, and mice, we can advance our understanding of the intricate roles of RA pathway molecules in retinal patterning and foveal progenitor development. Ultimately, such insights may contribute to unraveling the mechanisms underlying foveal specialization.

Supplementary Material

Refer to Web version on PubMed Central for supplementary material.

Acknowledgments

We want to thank all members of the La Torre and Simó laboratories for their helpful insights. We also want to thank Drs. Nadean Brown, Tom Glaser, and Nick Marsh-Armstrong for their valuable comments. This study was supported by NIH (R0EY026942; ALT), the California National Primate Research Center base operating grant (P51-OD011107), and a Pilot project grant supported by the Departments of Physiology and Cell Biology and Human Anatomy (to ALT and AFT). We also benefited from the use of the National Eye Institute Core Facilities (supported by P30 EY012576). *In vivo* sonographic imaging was performed by instrumentation obtained through an NIH S10 High-End Instrumentation grant to A.F.T (S10-OD016261).

References

Amamoto R, Garcia MD, West ER, Choi J, Lapan SW, Lane EA, Perrimon N, Cepko CL, 2019. Probe-Seq enables transcriptional profiling of specific cell types from heterogeneous tissue by RNA-based isolation. Elife 8.

Baden T, 2020. Vertebrate vision: lessons from non-model species. Semin. Cell Dev. Biol. 106, 1–4. [PubMed: 32532616]

Bringmann A, Syrbe S, Gorner K, Kacza J, Francke M, Wiedemann P, Reichenbach A, 2018. The primate fovea: structure, function and development. Prog. Retin. Eye Res 66, 49–84. [PubMed: 29609042]

Brown NL, Kanekar S, Vetter ML, Tucker PK, Gemza DL, Glaser T, 1998. Math5 encodes a murine basic helix-loop-helix transcription factor expressed during early stages of retinal neurogenesis. Development 125, 4821–4833. [PubMed: 9806930]

Brzezinski J.A.t., Prasov L, Glaser T, 2012. Math5 defines the ganglion cell competence state in a subpopulation of retinal progenitor cells exiting the cell cycle. Dev. Biol. 365, 395–413. [PubMed: 22445509]

Buenaventura DF, Corseri A, Emerson MM, 2019. Identification of genes with enriched expression in early developing mouse cone photoreceptors. Invest. Ophthalmol. Vis. Sci. 60, 2787–2799. [PubMed: 31260032]

Clark BS, Stein-O'Brien GL, Shiau F, Cannon GH, Davis-Marcisak E, Sherman T, Santiago CP, Hoang TV, Rajaii F, James-Esposito RE, Gronostajski RM, Fertig EJ, Goff LA, Blackshaw S, 2019. Single-cell RNA-seq analysis of retinal development identifies NFI factors as regulating mitotic exit and late-born cell specification. Neuron 102, 1111–1126 e1115. [PubMed: 31128945]

Cornish EE, Madigan MC, Natoli R, Hales A, Hendrickson AE, Provis JM, 2005. Gradients of cone differentiation and FGF expression during development of the foveal depression in macaque retina. Vis. Neurosci. 22, 447–459. [PubMed: 16212702]

Curcio CA, Allen KA, 1990. Topography of ganglion cells in human retina. J. Comp. Neurol. 300, 5–25. [PubMed: 2229487]

Curcio CA, Sloan KR Jr., Packer O, Hendrickson AE, Kalina RE, 1987. Distribution of cones in human and monkey retina: individual variability and radial asymmetry. Science 236, 579–582. [PubMed: 3576186]

Curcio CA, Sloan KR, Kalina RE, Hendrickson AE, 1990. Human photoreceptor topography. J. Comp. Neurol. 292, 497–523. [PubMed: 2324310]

da Silva S, Cepko CL, 2017. Fgf8 expression and degradation of retinoic acid are required for patterning a high-acuity area in the retina. Dev. Cell 42, 68–81 e66. [PubMed: 28648799]

Delaunay K, Khamsy L, Kowalczuk L, Moulin A, Nicolas M, Zografos L, Lassiaz P, Behar-Cohen F, 2020. Glial cells of the human fovea. Mol. Vis. 26, 235–245. [PubMed: 32280188]

Dowling JE, 1987. The Retina: an Approachable Part of the Brain. Harvard University Press.

Dyer MA, Martins R, da Silva Filho M, Muniz JA, Silveira LC, Cepko CL, Finlay BL, 2009. Developmental sources of conservation and variation in the evolution of the primate eye. Proc. Natl. Acad. Sci. U. S. A. 106, 8963–8968. [PubMed: 19451636]

Finkbeiner C, Ortuno-Lizaran I, Sridhar A, Hooper M, Petter S, Reh TA, 2022. Single-cell ATAC-seq of fetal human retina and stem-cell-derived retinal organoids shows changing chromatin landscapes during cell fate acquisition. Cell Rep. 38, 110294. [PubMed: 35081356]

Fishman ES, Louie M, Miltner AM, Cheema SK, Wong J, Schlaeger NM, Moshiri A, Simo S, Tarantal AF, La Torre A, 2021. MicroRNA signatures of the developing primate fovea. Front. Cell Dev. Biol. 9, 654385. [PubMed: 33898453]

Gariano RF, Provis JM, Hendrickson AE, 2000. Development of the foveal avascular zone. Ophthalmology 107, 1026.

Gass JD, 1999. Muller cell cone, an overlooked part of the anatomy of the fovea centralis: hypotheses concerning its role in the pathogenesis of macular hole and foveomacualr retinoschisis. Arch. Ophthalmol. 117, 821–823. [PubMed: 10369597]

Hendrickson A, 1992. A morphological comparison of foveal development in man and monkey. Eye 6 (Pt 2), 136–144. [PubMed: 1624035]

Hendrickson A, Kupfer C, 1976. The histogenesis of the fovea in the macaque monkey. Invest. Ophthalmol. Vis. Sci. 15, 746–756. [PubMed: 822712]

Hendrickson A, Possin D, Vajzovic L, Toth CA, 2012. Histologic development of the human fovea from midgestation to maturity. Am. J. Ophthalmol. 154, 767–778 e762. [PubMed: 22935600]

Hendrickson AE, Yuodelis C, 1984. The morphological development of the human fovea. Ophthalmology 91, 603–612. [PubMed: 6462623]

Holt CE, Bertsch TW, Ellis HM, Harris WA, 1988. Cellular determination in the Xenopus retina is independent of lineage and birth date. Neuron 1, 15–26. [PubMed: 3272153]

Hoshino A, Ratnapriya R, Brooks MJ, Chaitankar V, Wilken MS, Zhang C, Starostik MR, Gieser L, La Torre A, Nishio M, Bates O, Walton A, Bermingham-McDonogh O, Glass IA, Wong ROL, Swaroop A, Reh TA, 2017. Molecular anatomy of the developing human retina. Dev. Cell 43, 763–779 e764. [PubMed: 29233477]

Kolb H, 1995. Simple anatomy of the retina. In: Kolb H, Fernandez E, Nelson R (Eds.), Webvision: the Organization of the Retina and Visual System. Salt Lake City (UT).

Kolb H, Nelson RF, Ahnelt PK, Ortuno-Lizaran I, Cuenca N, 1995. The architecture of the human fovea. In: Kolb H, Fernandez E, Nelson R (Eds.), Webvision: the Organization of the Retina and Visual System. Salt Lake City (UT).

La Vail MM, Rapaport DH, Rakic P, 1991. Cytogenesis in the monkey retina. J. Comp. Neurol. 309, 86–114. [PubMed: 1894769]

Lahne MYT, MacDonald RB, 2023. Retinoic acid siganling in the developing zebrafish high acuity zone. Invest. Ophthalmol. Vis. Sci. 64.

Lee DA, Andreev A, Truong TV, Chen A, Hill AJ, Oikonomou G, Pham U, Hong YK, Tran S, Glass L, Sapin V, Engle J, Fraser SE, Prober DA, 2017. Genetic and neuronal regulation of sleep by neuropeptide VF. Elife 6.

Lu Y, Shiau F, Yi W, Lu S, Wu Q, Pearson JD, Kallman A, Zhong S, Hoang T, Zuo Z, Zhao F, Zhang M, Tsai N, Zhuo Y, He S, Zhang J, Stein-O'Brien GL, Sherman TD, Duan X, Fertig EJ, Goff LA, Zack DJ, Handa JT, Xue T, Bremner R, Blackshaw S, Wang X, Clark BS, 2020. Single-cell analysis of human retina identifies evolutionarily conserved and species-specific mechanisms controlling development. Dev. Cell 53, 473–491 e479. [PubMed: 32386599]

Marsh-Armstrong N, McCaffery P, Gilbert W, Dowling JE, Drager UC, 1994. Retinoic acid is necessary for development of the ventral retina in zebrafish. Proc. Natl. Acad. Sci. U. S. A. 91, 7286–7290. [PubMed: 8041782]

Miesfeld JB, Glaser T, Brown NL, 2018. The dynamics of native Atoh7 protein expression during mouse retinal histogenesis, revealed with a new antibody. Gene Expr. Patterns 27, 114–121. [PubMed: 29225067]

Mitkus M, Olsson P, Toomey MB, Corbo JC, Kelber A, 2017. Specialized photoreceptor composition in the raptor fovea. J. Comp. Neurol. 525, 2152–2163. [PubMed: 28199005]

Okada M, Erickson A, Hendrickson A, 1994. Light and electron microscopic analysis of synaptic development in Macaca monkey retina as detected by immunocytochemical labeling for the synaptic vesicle protein, SV2. J. Comp. Neurol. 339, 535–558. [PubMed: 8144745]

Peng YR, Shekhar K, Yan W, Herrmann D, Sappington A, Bryman GS, van Zyl T, Do MTH, Regev A, Sanes JR, 2019. Molecular classification and comparative taxonomics of foveal and peripheral cells in primate retina. Cell 176, 1222–1237 e1222. [PubMed: 30712875]

Picaud S, Dalkara D, Marazova K, Goureau O, Roska B, Sahel JA, 2019. The primate model for understanding and restoring vision. Proc. Natl. Acad. Sci. U. S. A. 116, 26280–26287. [PubMed: 31871177]

Provis JM, Diaz CM, Dreher B, 1998. Ontogeny of the primate fovea: a central issue in retinal development. Prog. Neurobiol. 54, 549–580. [PubMed: 9550191]

Provis JM, Hendrickson AE, 2008. The foveal avascular region of developing human retina. Arch. Ophthalmol. 126, 507–511. [PubMed: 18413520]

Provis JM, Sandercoe T, Hendrickson AE, 2000. Astrocytes and blood vessels define the foveal rim during primate retinal development. Invest. Ophthalmol. Vis. Sci. 41, 2827–2836. [PubMed: 10967034]

Rakic P, Riley KP, 1983. Overproduction and elimination of retinal axons in the fetal rhesus monkey. Science 219, 1441–1444. [PubMed: 6828871]

Rapaport DH, Wong LL, Wood ED, Yasumura D, LaVail MM, 2004. Timing and topography of cell genesis in the rat retina. J. Comp. Neurol. 474, 304–324. [PubMed: 15164429]

Rasys AM, Pau SH, Irwin KE, Luo S, Kim HQ, Wahle MA, Trainor PA, Menke DB, Lauderdale JD, 2021. Ocular elongation and retraction in foveated reptiles. Dev. Dynam. 250, 1584–1599.

Roll B, 2001. Retina of Bouton's skink (Reptilia, Scincidae): visual cells, fovea, and ecological constraints. J. Comp. Neurol. 436, 487–496. [PubMed: 11447591]

Sakai Y, Luo T, McCaffery P, Hamada H, Drager UC, 2004. CYP26A1 and CYP26C1 cooperate in degrading retinoic acid within the equatorial retina during later eye development. Dev. Biol. 276, 143–157. [PubMed: 15531370]

Sannan NS, Shan X, Gregory-Evans K, Kusumi K, Gregory-Evans CY, 2018. Anolis carolinensis as a model to understand the molecular and cellular basis of foveal development. Exp. Eye Res. 173, 138–147. [PubMed: 29775563]

Sidman R, 1961. Histogenesis of the Mouse Retina Studied with Thymidine-H3.

Sjostrand J, Olsson V, Popovic Z, Conradi N, 1999. Quantitative estimations of foveal and extra-foveal retinal circuitry in humans. Vis. Res. 39, 2987–2998. [PubMed: 10664798]

Sridhar A, Hoshino A, Finkbeiner CR, Chitsazan A, Dai L, Haugan AK, Eschenbacher KM, Jackson DL, Trapnell C, Bermingham-McDonogh O, Glass I, Reh TA, 2020. Single-cell transcriptomic comparison of human fetal retina, hPSC-derived retinal organoids, and long-term retinal cultures. Cell Rep. 30, 1644–1659 e1644. [PubMed: 32023475]

Tarantal AF, 2005. Ultrasound imaging in rhesus (Macaca mulatta) and long-tailed (Macaca fascicularis) Macaques. Reproductive and research applications. In: W.-C. S (Ed.), Laboratory Primate Ch. 20. Elsevier Academic Press, pp. 315–317.

Thomas ED, Timms AE, Giles S, Harkins-Perry S, Lyu P, Hoang T, Qian J, Jackson VE, Bahlo M, Blackshaw S, Friedlander M, Eade K, Cherry TJ, 2022. Cell-specific cis-regulatory elements and mechanisms of non-coding genetic disease in human retina and retinal organoids. Dev. Cell 57, 820–836 e826. [PubMed: 35303433]

Townes-Anderson E, Raviola G, 1981. The formation and distribution of intercellular junctions in the rhesus monkey optic cup: the early development of the cilio-iridic and sensory retinas. Dev. Biol. 85, 209–232. [PubMed: 7250513]

Turner DL, Cepko CL, 1987. A common progenitor for neurons and glia persists in rat retina late in development. Nature 328, 131–136. [PubMed: 3600789]

Vazquez-Chona FR, Clark AM, Levine EM, 2009. Rlbp1 promoter drives robust Muller glial GFP expression in transgenic mice. Invest. Ophthalmol. Vis. Sci. 50, 3996–4003. [PubMed: 19324864]

Viets K, Eldred K, Johnston RJ Jr., 2016. Mechanisms of photoreceptor patterning in vertebrates and invertebrates. Trends Genet. 32, 638–659. [PubMed: 27615122]

Voigt AP, Whitmore SS, Flamme-Wiese MJ, Riker MJ, Wiley LA, Tucker BA, Stone EM, Mullins RF, Scheetz TE, 2019. Molecular characterization of foveal versus peripheral human retina by single-cell RNA sequencing. Exp. Eye Res. 184, 234–242. [PubMed: 31075224]

Wagner E, McCaffery P, Drager UC, 2000. Retinoic acid in the formation of the dorsoventral retina and its central projections. Dev. Biol. 222, 460–470. [PubMed: 10837133]

Wallace VA, 2011. Concise review: making a retina–from the building blocks to clinical applications. Stem Cell. 29, 412–417.

Wikler KC, Rakic P, 1991. Relation of an array of early-differentiating cones to the photoreceptor mosaic in the primate retina. Nature 351, 397–400. [PubMed: 1827876]

Yamada E, 1969. Some structural features of the fovea centralis in the human retina. Arch. Ophthalmol. 82, 151–159. [PubMed: 4183671]

Yamagata M, Yan W, Sanes JR, 2021. A cell atlas of the chick retina based on single-cell transcriptomics. Elife 10.

Yan W, Peng YR, van Zyl T, Regev A, Shekhar K, Juric D, Sanes JR, 2020. Cell atlas of the human fovea and peripheral retina. Sci. Rep. 10, 9802. [PubMed: 32555229]

Yi W, Lu Y, Zhong S, Zhang M, Sun L, Dong H, Wang M, Wei M, Xie H, Qu H, Peng R, Hong J, Yao Z, Tong Y, Wang W, Ma Q, Liu Z, Ma Y, Li S, Yin C, Liu J, Ma C, Wang X, Wu Q, Xue T, 2021. A single-cell transcriptome atlas of the aging human and macaque retina. Natl. Sci. Rev 8, nwaa179. [PubMed: 34691611]

Yoshimatsu T, Schroder C, Nevala NE, Berens P, Baden T, 2020. Fovea-like photoreceptor specializations underlie single UV cone driven prey-capture behavior in zebrafish. Neuron 107, 320–337 e326. [PubMed: 32473094]

Young RW, 1985. Cell differentiation in the retina of the mouse. Anat. Rec. 212, 199–205. [PubMed: 3842042]

Yuodelis C, Hendrickson A, 1986. A qualitative and quantitative analysis of the human fovea during development. Vis. Res. 26, 847–855. [PubMed: 3750868]

Zhang X, Leavey P, Appel H, Makrides N, Blackshaw S, 2023. Molecular mechanisms controlling vertebrate retinal patterning, neurogenesis, and cell fate specification. Trends Genet. 39, 736–757. [PubMed: 37423870]

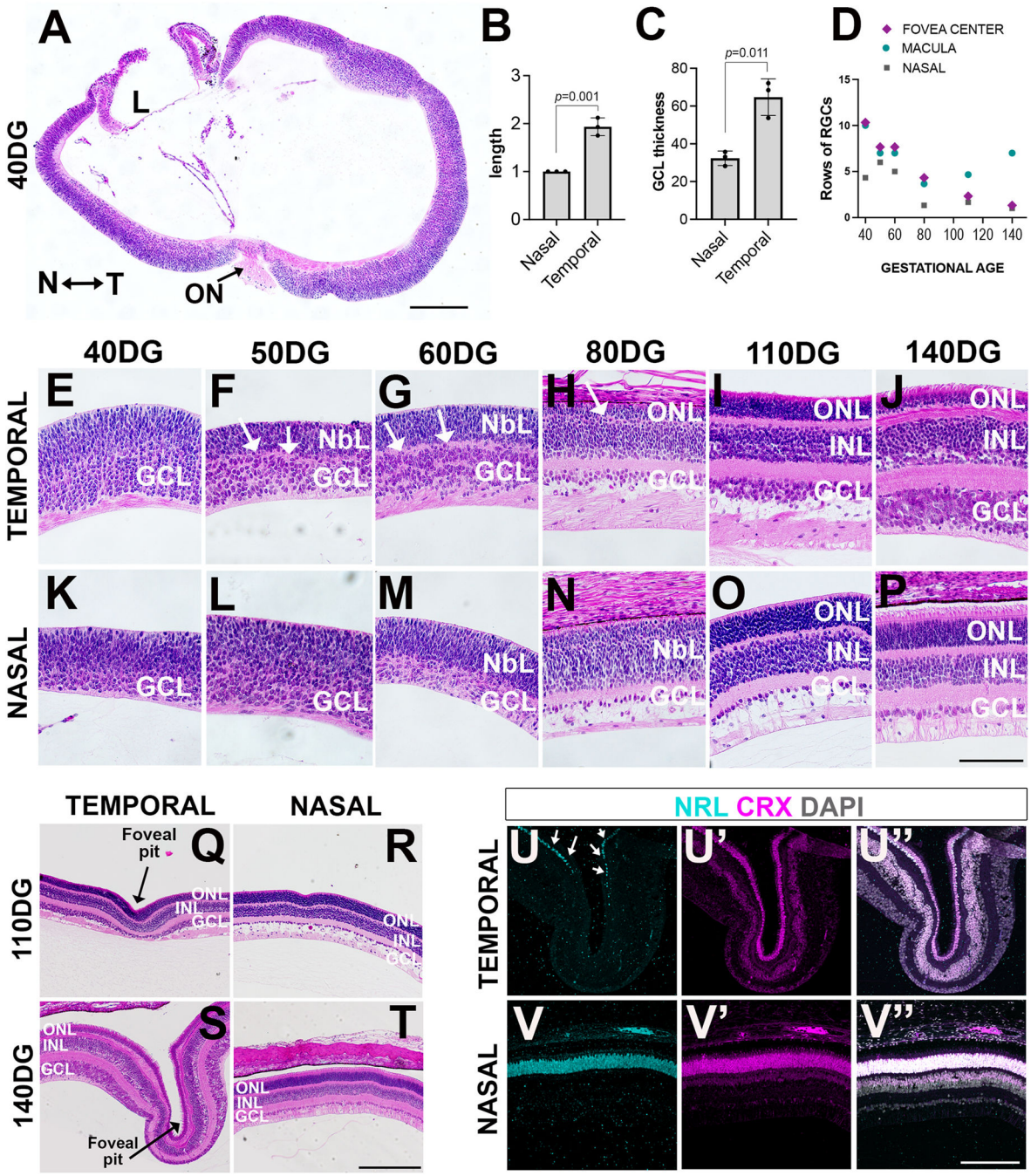

Fig. 1.

The foveal region is developmentally advanced **A.** Hematoxylin and eosin (H&E) staining of a paraffin-embedded section of the eye at 40 days gestational age which shows a larger temporal side. **B-C.** Quantifications of retinal length (relative to the nasal side) and GCL thickness (microns) at 40 days gestational age. Mean ± SEM. P-values were obtained using Student's T-test. **D.** The number of rows of RGCs in the center of the fovea, macula (tissue surrounding the center of the fovea), and nasal regions was quantified at different gestational ages. **E-P.** H&E staining (40–140 days gestational age). White arrows (F-H) indicate the

presence of plexiform layers in the temporal side. **Q-R.** Development of the foveal pit is observed in the temporal side from ~110 days gestational age. **S-T**. Mature foveal pit observed near term at 140 days gestational age. **U-V''.** The 140 days gestational age sections were immunostained with NRL (cyan), CRX (magenta), and counterstained with DAPI (grey). Arrows in U indicate NRL + cells at the edge of the fovea but note that while there are CRX + photoreceptors, there are no NRL + rods in the center of the fovea. Scale bars: 250 μm in A, 100 μm in O, 200 μm in S and U. DG: days gestational age, ON: optic nerve, GCL: ganglion cell layer, NbL: neuroblastic layer, ONL: outer nuclear layer, INL: inner nuclear layer.

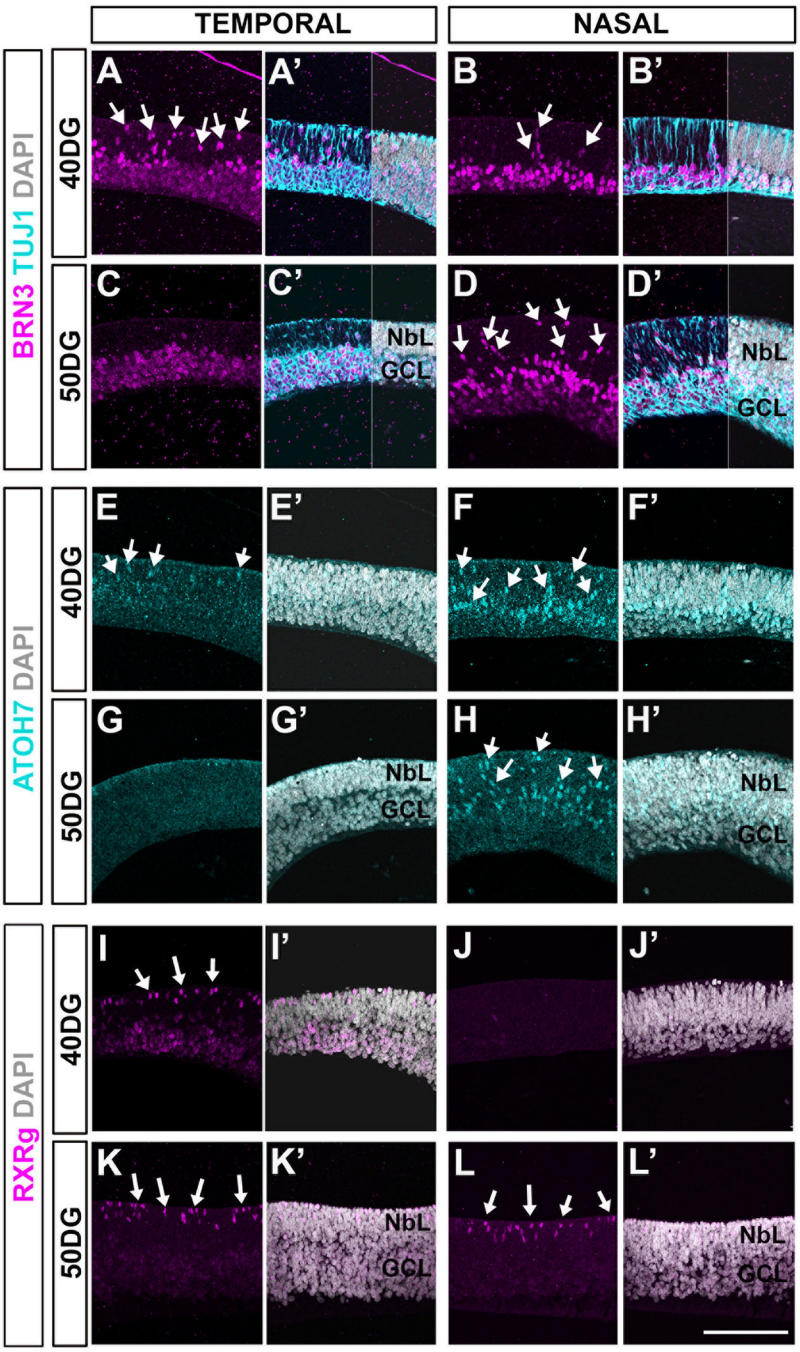

Fig. 2.

Early neurogenesis in the developing rhesus monkey retina **A-D'.** RGCs are stained with BRN3 (magenta), TUJ1 (cyan), and counterstained with DAPI (grey) at the gestational ages indicated (40–50 days gestational age). Arrows indicate newly-born RGCs located in the apical side of the retina. **E-H'.** ATOH7 is labeled in cyan (arrows) and the retinas are counterstained with DAPI (grey). Note the absence of ATOH7+ cells in the temporal retina at 50 days gestational age (G-G′). **I-L'**. RXRgamma is labeled in magenta (arrows) and the

retinas are counterstained with DAPI (grey). Scale bar: 100 μm. DG: days gestational age, NbL: neuroblastic layer, GCL: ganglion cell layer.

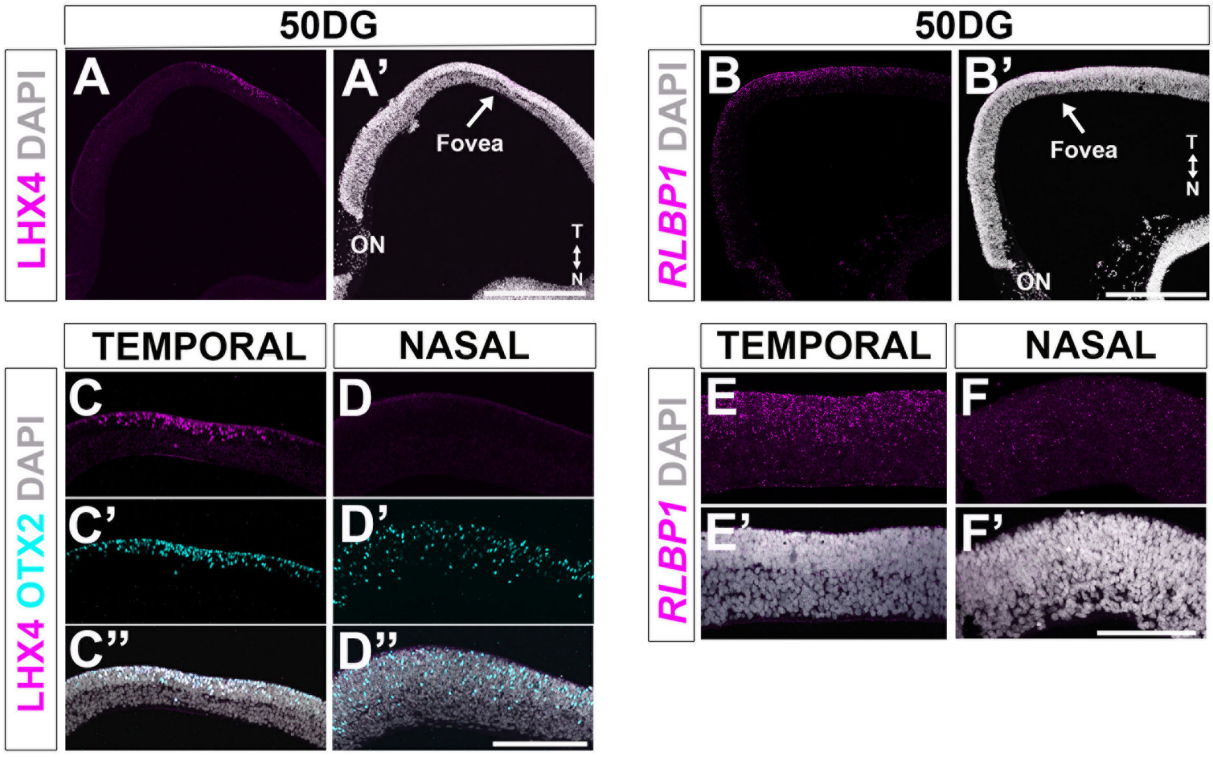

Fig. 3.

Late cell types are detected in the foveal anlage at 50 days gestational age **A-A'.** Low magnification image of a 50 days gestational age retina showed the expression of LHX4 protein (magenta). **B-B'.** RNAscope *in situ* hybridization for *RLBP1* (magenta) showed enriched expression in the temporal retina at 50 days gestational age. **C-D-D''.** LHX4+ cells (magenta) colocalize with OTX2 (cyan). Note the restricted expression of LHX4 in the temporal retina. E-F'. *RLBP1* exhibits low levels of expression throughout the retina but it is highly expressed in the foveal region. In all cases, tissues have been counterstained with DAPI (grey). Scale bar: 250 μm in A′ and B′, 100 μm in D″ and F'.ON: optic nerve, T: temporal, N: nasal.

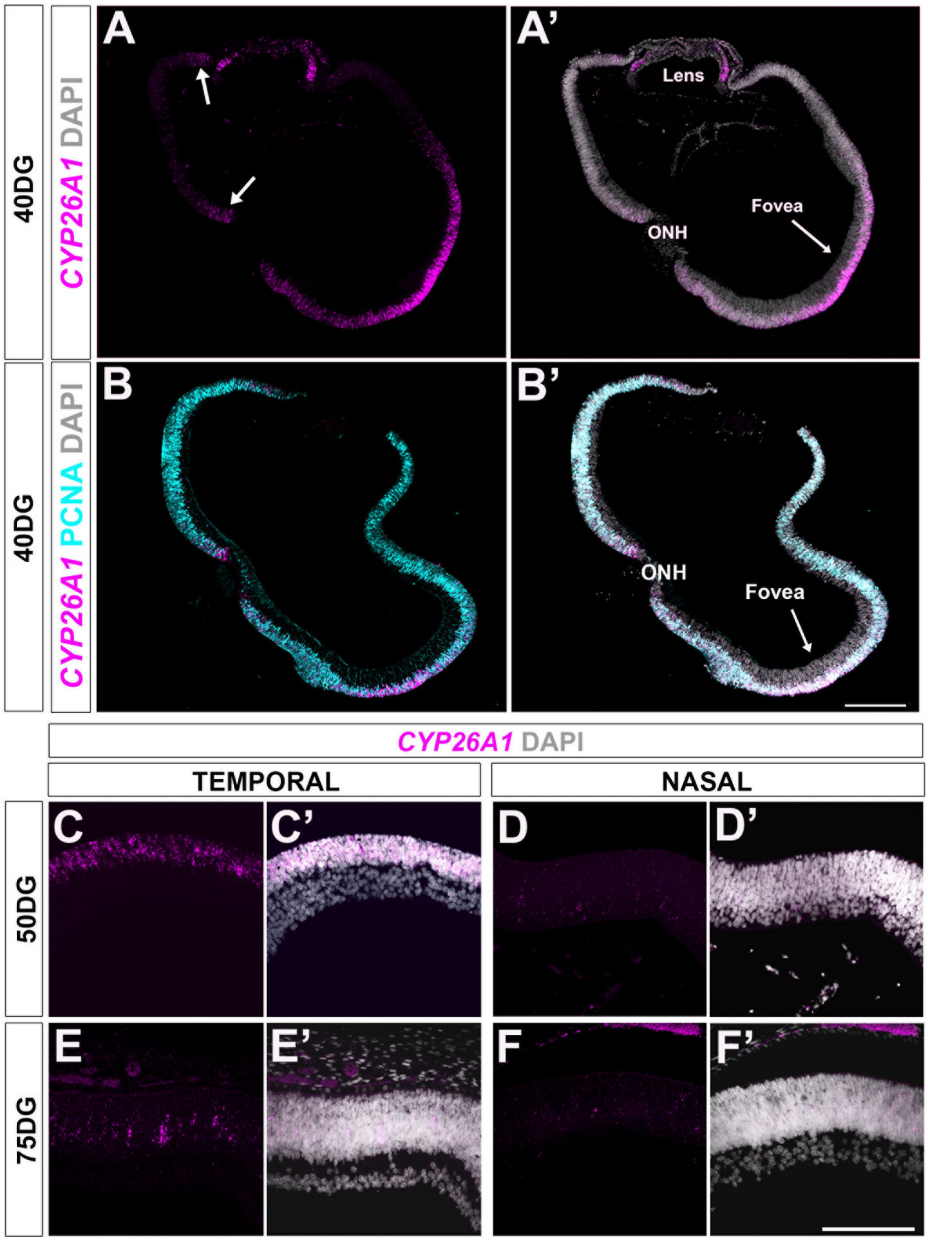

Fig. 4.

CYP26A1 is enriched in the progenitors of the fovea **A-A'.** RNAscope *in situ* hybridization for *CYP26A1* (magenta) at 40 days gestational age (DG) revealed enriched expression in the foveal region. Other regions (A, white arrows) such as the lens epithelium, the ciliary margin, and a patch of cells around the optic nerve also expressed *CYP26A1.* **B-B′** Colocalization between *CYP26A1* (magenta) and PCNA (cyan) is shown at 40 days gestational age. Retinas were counterstained with DAPI (grey). **C-F'.** Expression pattern of *CYP26A1* (magenta) in the temporal and nasal retina at indicated ages (50–70 days gestational age). Samples have been counterstained with DAPI (grey). Scale bars: 250 μm in B′, 100 μm in F'. ONH: optic nerve head.

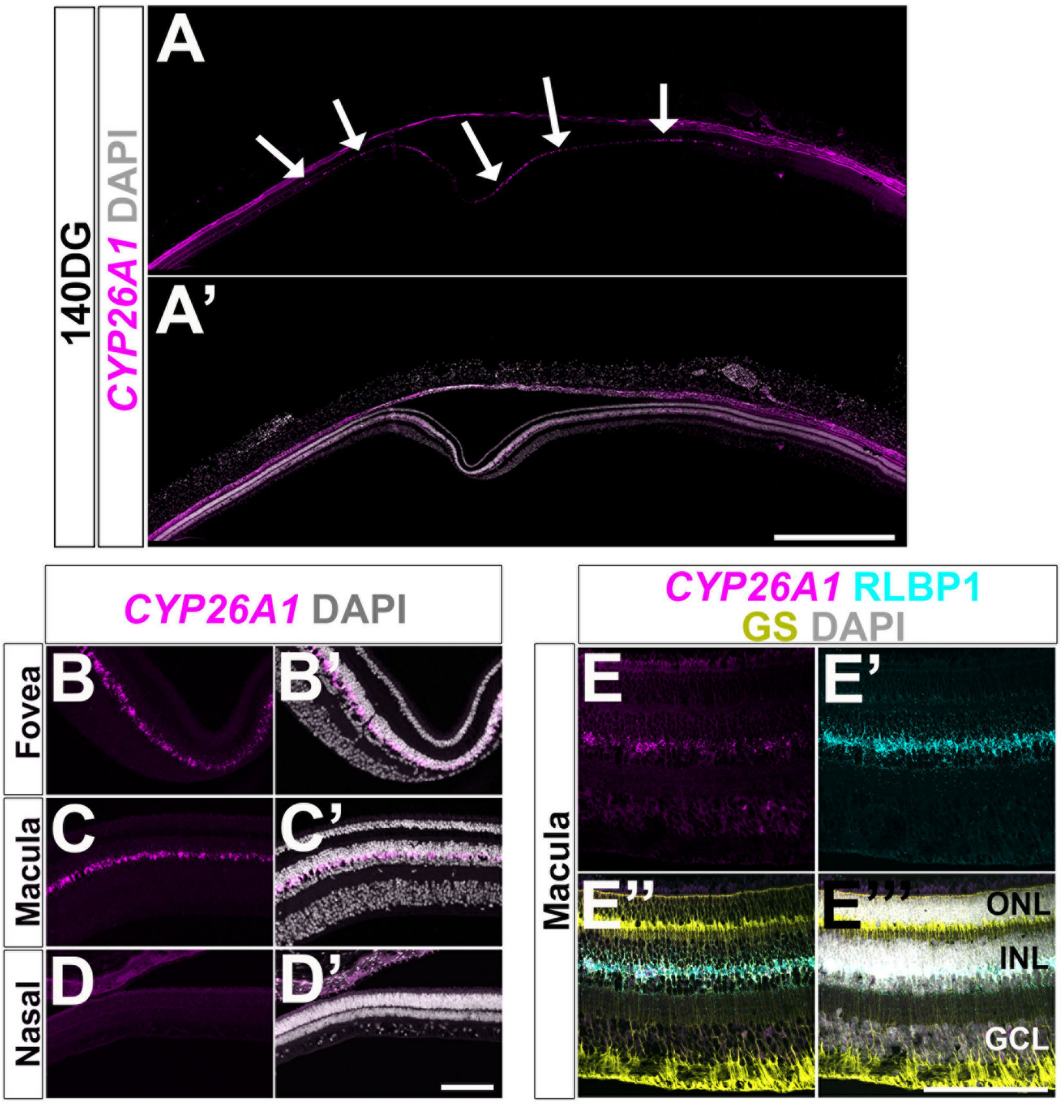

Fig. 5.

At later stages of gestation *CYP26A1* colocalizes with Müller glia cells **A-D'.** *In situ* hybridization for *CYP26A1* (magenta) at ~140 days gestational age (DG) showed expression in the center of the fovea and other macula regions (foveolar, fovea, and perifovea. Arrows in A) but not in the rest of the retina. **E-E‴**. The expression of *CYP26A1* (magenta) colocalizes with *RLBP1* (cyan) and GS (yellow). All tissues have been counterstained with DAPI (grey). Scale bars: 400 μm in A′, 150 μm in D′, 100 μm in E'.

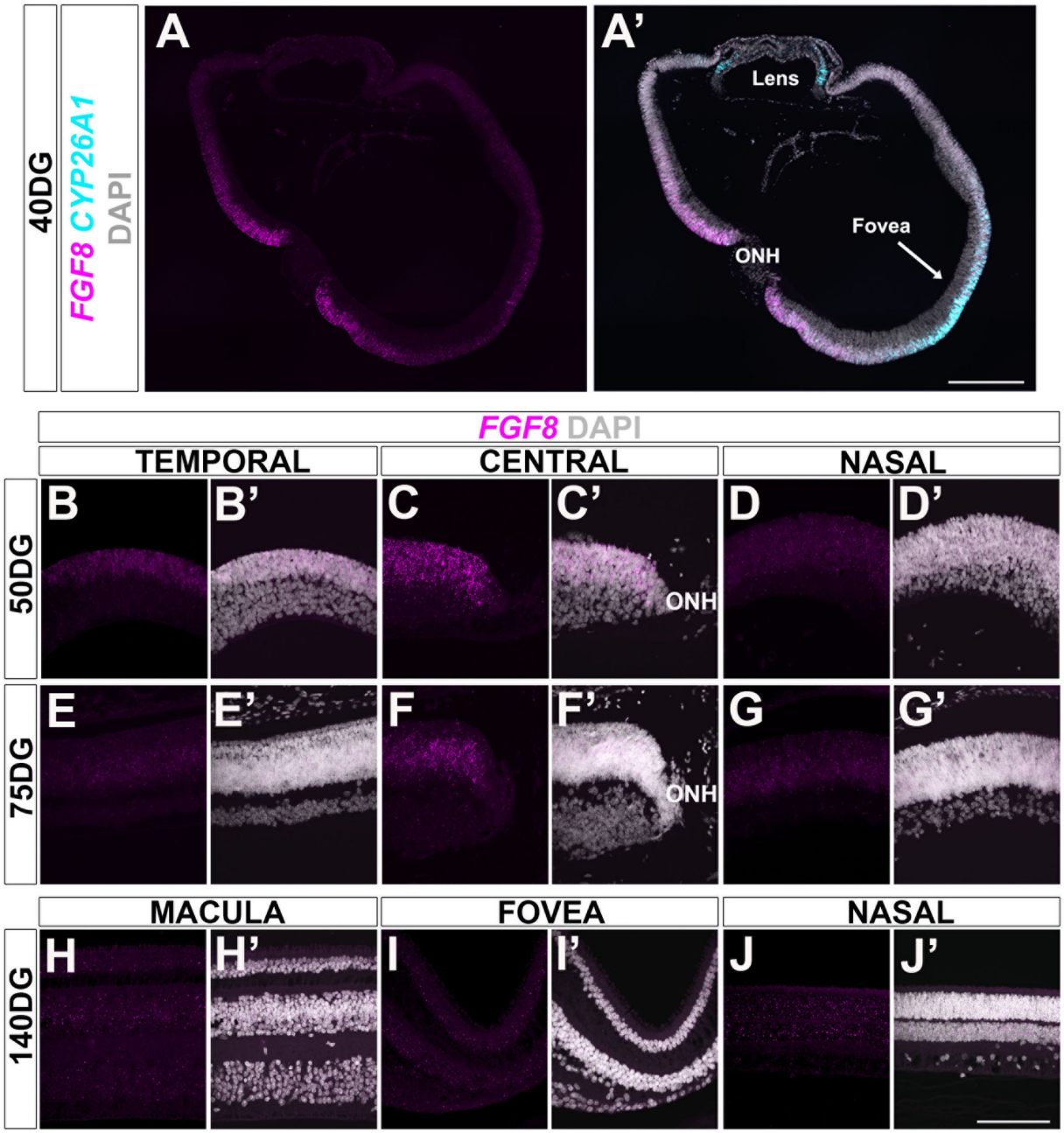

Fig. 6.

FGF8 is expressed in a central-to-periphery gradient in the developing rhesus monkey retina **A-A'.** *FGF8* (magenta) is highly expressed in the cells surrounding the optic nerve and its expression exhibits a gradient that extends peripherally in both temporal and nasal sides of the retina. This expression pattern does not mimic *CYP26A1* expression (cyan, A′). **B-G'.** The expression pattern of *FGF8* (magenta) at 50 and 75 days gestational age show a similar pattern with higher expression in the central part of the retina. Samples were counterstained with DAPI (grey) **H-J'.** At later time points, *FGF8* is only expressed at low levels in both the ONL2019 and INL. Scale bars: 250 μm in A′, 100 μm in J'. ONH: optic nerve head.

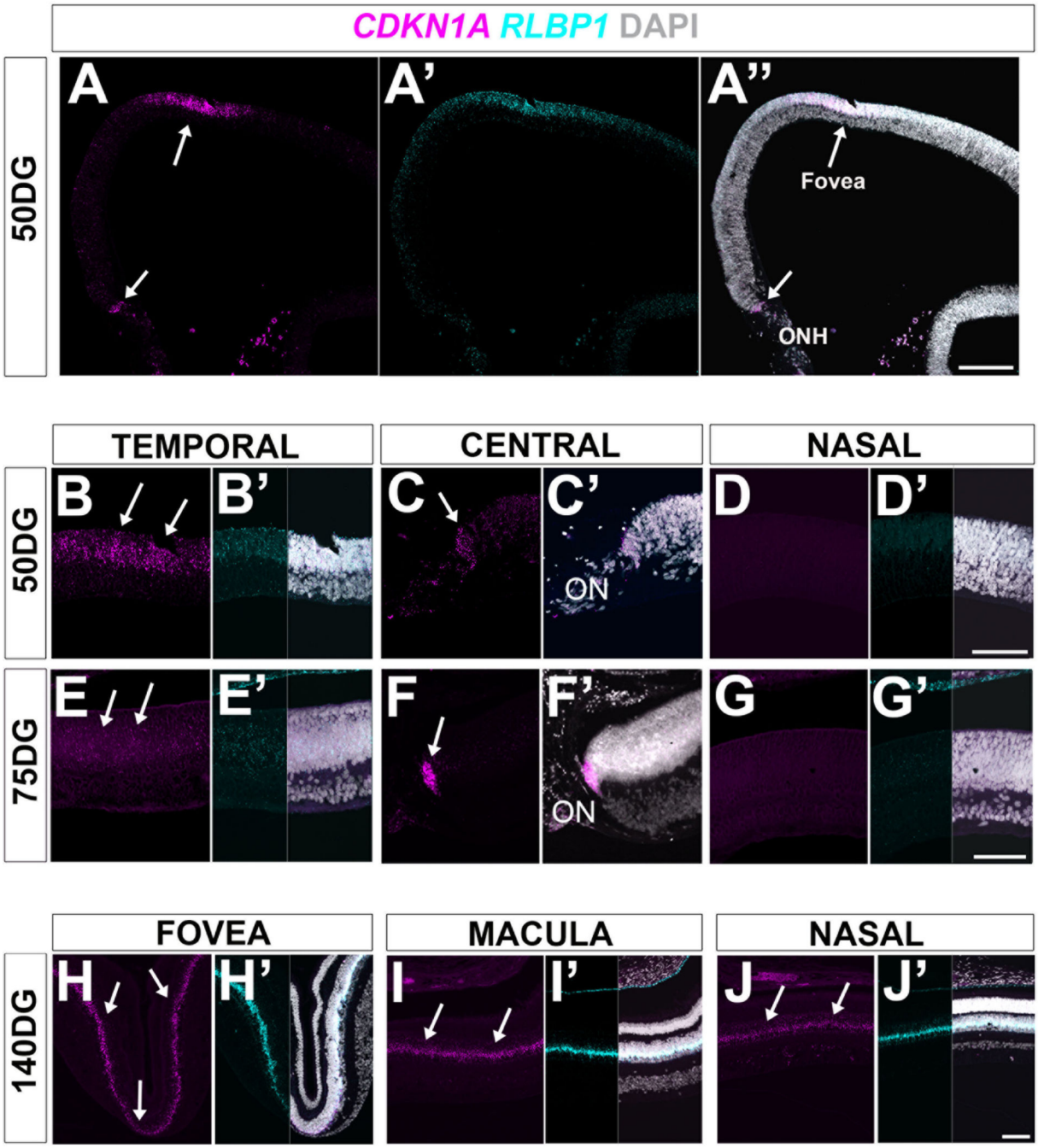

Fig. 7.

CDKN1A is expressed by Müller glia cells **A-A".** RNAscope *in situ* hybridization for *CDKN1A* (magenta) revealed enriched expression in the foveal region and optic nerve head cells at 50 days gestational age (arrows in A). The enriched expression at the center of the fovea colocalizes with high levels of *RLBP1* (cyan). **B-G'.** Expression of *CDKN1A* (magenta) and *RLBP1* (cyan) in different regions of the retina at 50 and 75 days gestational age. Arrows indicate enriched expression in the temporal retina and optic nerve head. **H-J'.** In the late third trimester (~140 days gestation) *CDKN1A* (magenta) was shown to be

expressed by *RLBP1*+ cells (cyan) throughout all regions of the retina. Scale bars: 250 μm in A″, 70 μm in D′, G′, and J'. ONH: optic nerve head, ON: optic nerve.

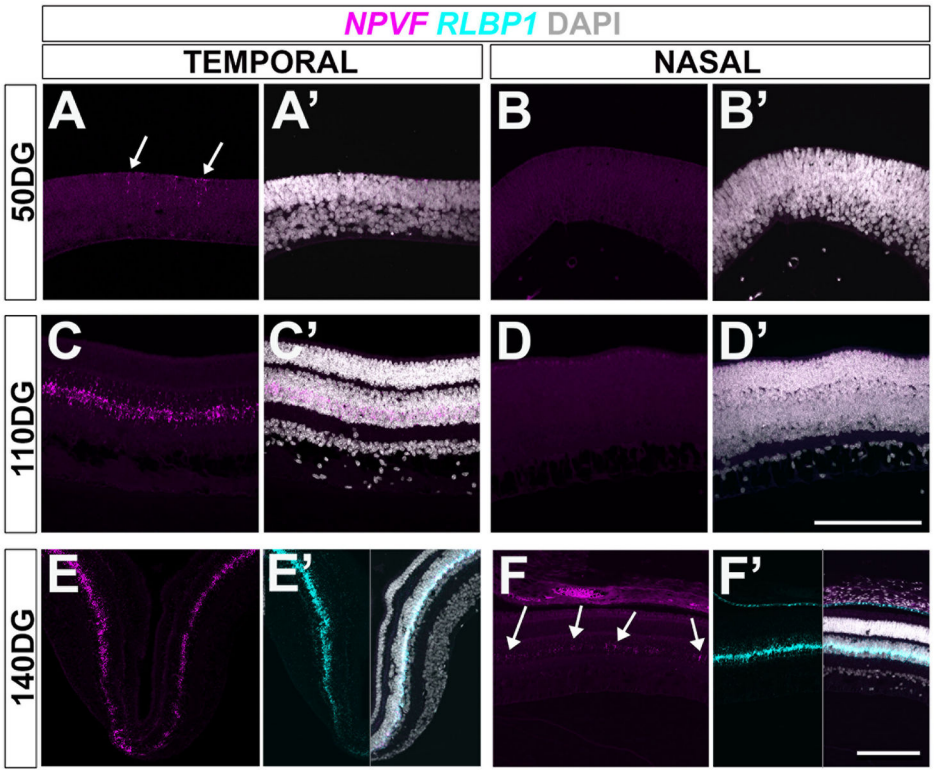

Fig. 8.

NPVF is expressed by Müller glia cells at slightly later times in development A-B'. A-B'. *NPVF* (magenta) was only weakly expressed by some cells at the center of the foveal anlage (arrows in A) at 50 days gestational age (late first trimester). C-D'. By 110 days gestational age (early third trimester), the expression of *NPVF* had extended throughout the temporal side of the retina. E-F'. At 140 days gestational age (late third trimester), the expression of *NPVF* can be faintly detected in the nasal retina (arrows in F). The cells that expressed *NPV*F also expressed *RLBP1* (cyan). Scale bar: 100 μm in D′, 150 μm in F'.

Table 1

Summary of morphological characteristics and neurogenesis of the fovea at different periods of gestation.

Gestation Day	% Gestation	Foveal development and morphology
40	24	Thicker GCL; early cell types are produced
50	30	IPL appears; cones form a continuous row; late-born cells are present in the foveal center
60	36	Clear IPL; neurogenesis is done in the foveal center
70	44	OPL appears
110	65	Shallow foveal pit; OS appear
140	86	GCL is 2 cells thick; 2 layer of elongated cones with IS and OS

Table 2

Expression patterns of *CYP26A1, FGF8, CDKN1A,* and *NPVF* in the rhesus monkey eye. Very low (+/−), low (+), moderate (++), high (+++), and very high (++++) levels of expression. No detectable expression is indicated (−). N/ A (not applicable) indicating that the corresponding areas were not defined at that developmental stage.

	DG 40	DG 50	DG 70	DG 110	DG 140–145
CYP26A1					
RETINA					
RPCs temporal/fovea	++++	++++	n/a	n/a	n/a
RPCs nasal	+	+	−/+	−/+	n/a
RPCs central	++	++	+	-	n/a
RGCs	-	−/+	−/+	-	-
Photoreceptors	-	-	-	-	-
Horizontal cells			-	-	-
Amacrine cells	n/a		-	-	-
Bipolar cells	n/a		-	-	-
Müller glia	n/a	++	++*	++++*	++++*
ONH	-	-	-	-	-
Optic nerve	-	-	−/+	−/+	−/+
RPE	-	-	-	-	-
Ciliary margin zone	+	+	+	+	+
LENS					
Lens epithelium	++	++	++	++	
Bow region			-	-	
Lens fibers			-	-	
CORNEA	-	-	-	-	-
*Exclusively expressed in the macula					
FGF8					
RETINA					
RPCs temporal/fovea	++	++	n/a	n/a	n/a
RPCs nasal	+	+	+	+	n/a
RPCs central	++++	++++	++++	++	n/a
RGCs	-	-	-	−/+	−/+
Photoreceptors			+	+	+
Horizontal cells		−/+	−/+	−/+	−/+
Amacrine cells	n/a	−/+	−/+	+	+
Bipolar cells	n/a	−/+	−/+	+	+
Müller glia	n/a		+	+	+
ONH	+	+	+	+	+
Optic nerve	-	-	-	-	-
RPE	-	-	-	-	-

	DG 40	DG 50	DG 70	DG 110	DG 140–145
Ciliary margin zone	-	-	-	-	-
LENS					
Lens epithelium	-	-	-	-	
Bow region			-	-	
Lens fibers			-	-	
CORNEA	-	-	-	-	-
NPVF					
RETINA					
RPCs temporal/fovea	-	-	n/a	n/a	n/a
RPCs nasal	-	-			n/a
RPCs central	-	-	-	-	n/a
RGCs	-	-	-	-	-
Photoreceptors	-	-	-	-	-
Horizontal cells			-	-	-
Amacrine cells	n/a	-	-	-	-
Bipolar cells	n/a	-	-	-	-
Müller glia	n/a	-	+	++	+++
ONH	-	-	-	-	-
Optic nerve	-	-	-	-	-
RPE	-	-	−/+	−/+	−/+
Ciliary margin zone	-	-	-	-	-
LENS					
Lens epithelium	++	+	−/+	−/+	
Bow region			-	-	
Lens fibers			-	-	
CORNEA					
CDKN1A					
RETINA					
RPCs temporal/fovea	-	-	n/a	n/a	n/a
RPCs nasal	-	-	-		n/a
RPCs central	-	-	-	-	n/a
RGCs	-	-	-	-	-
Photoreceptors	-	-	-	-	-
Horizontal cells		-	-	-	-
Amacrine cells	n/a	-	-	-	-
Bipolar cells	n/a	-	-	-	-
Müller glia	n/a	++	+++	+++	+++
ONH	++	++	+++	+++	+
Optic nerve	+	+	+	+	-
RPE	+/−	+/−	+/−	+/−	+/−
Ciliary margin zone	+/−	+/−	+/−	+/−	+/−
LENS					

	DG 40	DG 50	DG 70	DG 110	DG 140–145
Lens epithelium	++	+	-	-	
Bow region			-	-	
Lens fibers			-	-	
CORNEA	++	+	+	+	+

(*) indicates exclusively expressed in the macula but not in other retinal regions. Empty table cells: expression not analyzed.